Fuel 331 (2023) 125876

Contents lists available at ScienceDirect

Fuel

journal homepage: www.elsevier.com/locate/fuel

Full Length Article

Experiments and modeling of the temperature profile of turbulent diffusion flames with large ullage heights

Jinlong Zhao [a], Xiang Zhang [a], Guangheng Song [a], Hong Huang [b], Jianping Zhang [c,*]

[a] School of Emergency Management & Safety Engineering, China University of Mining & Technology (Beijing), Beijing, China
[b] Institute of Public Safety Research, Department of Engineering Physics, Tsinghua University, Beijing, China
[c] FireSERT, Belfast School of Architecture and the Built Environment, Ulster University, Newtownabbey BT37 0QB, United Kingdom

ARTICLE INFO

Keywords:
Turbulent diffusion flame
Ullage height
Axial temperature
Virtual origin
Global temperature models

ABSTRACT

In the last decades, several major fire accidents involving storage tanks occurred, particularly for the tanks with a low fuel level (large ullage height). In case of a tank fire, the axial temperature profile is affected by the ullage because of the restriction in air entrainment by the tank sidewall. This work is aimed at examining the temperature profile of turbulent diffusion flames with large ullage heights. A series of experiments were conducted with different ullage heights (h = 16–42 cm) and fuel supply rates. The temperature profiles both inside and outside the fuel tray were measured and analyzed. Five regions were identified based on flame intermittencies: namely 1) fuel vapor, 2) down-reaching intermittent flame, 3) continuous flame (down-reaching and upper flame), 4) upper intermittent flame and 5) buoyant plume. It was found that for a given fuel supply rate the length of the fuel vapor region increases linearly with the ullage height. The lengths of the fuel vapor and continuous flame regions both increase with the fuel supply rate, whereas that of the down-reaching intermittent flame region shows an opposite trend. Based on the experimental data and dimensionless analysis, new correlations for the virtual origin were proposed, which were then incorporated in the predictions of the temperature profiles in both upper and down-reaching flames. The present results could not only contribute to the understanding the effects of the ullage height on the axial temperature profile in storage fuel tank fires with large ullage heights but are also of practical importance in the thermal hazard assessment of fire accidents involving tank liquid fuels.

1. Introduction

With the rapid development of the world economy, liquid fuels remain one of the key energy sources and currently supplies about 30 % of the overall energy consumption around the world and will remain an indispensable part in the future [1]. In order to store large quantities of liquid fuels, storage tanks have been built and widely used [1,2]. In a liquid fuel storage tank, the ullage height (the distance between the fuel surface and the tank upper rim) is one of the key parameters affecting the flow structure and flame development in a fire accident. In recent years, several major fire accidents involving storage tanks occurred, particularly for the tanks with a low liquid level (large ullage height) [3]. Once the fuel is ignited, the flame base will move up due to restriction of air entrainment by the sidewall, resulting in a significant change of the flame temperature profile [4], which in turn can affect the evolution of the fire accident and determine the likelihood of fire escalation. On April 6, 2015, a major fire accident involving a liquid fuel storage tank occurred in Fujian, China [5]. Because of the large ullage height (h = 11 m), the flame entered the tank, resulting in the collapse of the sidewall and the occurrence of spill fires and eventually ignited three nearby storage tanks. The high temperature inside the tank also made it difficult to extinguish the fire because of the large upward momentum of the fire plume.

The axial (centerline) temperature in the fire plume of pool fires has been examined extensively [e.g., 6–10]. McCaffrey [6] conducted experiments using a natural gas burner (0.3 m^2) to investigate the axial temperature profile for heat release rates ($\dot{Q}$) ranging from 14.4 to 57.5 kW. Three distinguishing regions (continuous flame, intermittent flame and buoyant plume) were identified and the correlations between the axial temperature and $\dot{Q}$ was established. A similar correlation was also provided by Gong et al. for rectangular n-heptane pool fires with different aspect ratios (n = tray length/tray width, $1 \leq n \leq 14$) [7] and the aspect ratio was introduced to modify the temperature profile.

* Corresponding author.
E-mail address: j.zhang@ulster.ac.uk (J. Zhang).

https://doi.org/10.1016/j.fuel.2022.125876
Received 1 July 2022; Received in revised form 18 August 2022; Accepted 29 August 2022
Available online 12 September 2022

Nomenclature

D	tray diameter (m)
h	ullage height (m)
h^*	dimensionless ullage height (h/D)
L_{down}	down-reaching flame length (m)
L_{upper}	upper flame length (m)
L_{total}	total flame length (m)
Q	fuel supply flow rate (L/min)
$\dot{Q}$	heat release rate (kW)
$\dot{Q}_c$	convective heat release rate (kW)
$\dot{Q}_{upper}$	heat release rate for upper flame (kW)
$\dot{Q}_{down}$	heat release rate for down-reaching flame (kW)
$\dot{Q}^*$	dimensionless heat release rate
Z	local height (m)
Z_0	virtual origin (m)
Fr	Froude number
Fr_f	flame Froude number, in Eq. (9)
u	fire plume velocity (m/s)
u_s	velocity of the fuel ejected from the burner surface (m/s)
g	gravitational acceleration (m/s^2)
T_∞	ambient air temperature (K)
T_g	averaged surrounding gas temperature (K)
ΔT	excess temperature (above the ambient) (K)
ΔT_r	temperature measurement error (K)
$\overline{\Delta T_f}$	mean peak flame temperature rise (above the ambient) (K)
c_p	specific heat of air (kJ/kg·K)
S	air to fuel mass stoichiometric ratio
b_L	radius of the fire plume at the mean flame height (m)
k	thermal conductivity of the gas (W/(m·K)

Greek symbols

σ	Stefan-Boltzmann constant (W/(m^2·K^4)
α	entrainment rate coefficient, in Eq. (2)
ρ_∞	ambient air density (kg/m^3)
ρ_s	fuel density (kg/m^3)

Heskestad [8,9] introduced the virtual origin height Z_0 by considering air entrainment and found that the axial temperature in the fire plume varied as −3/5 power of Z-Z_0 (Z: local height). Hu et al. [10] experimentally studied the axial temperature profile of propane turbulent jet flames with diameters of 4–10 mm at two atmospheric pressures (0.64 and 1 atm). The virtual origin was used to modify the temperature predictions and the virtual origin height was correlated with a flame Froude number (Fr_f) in a 2/5 power law function. These studies showed

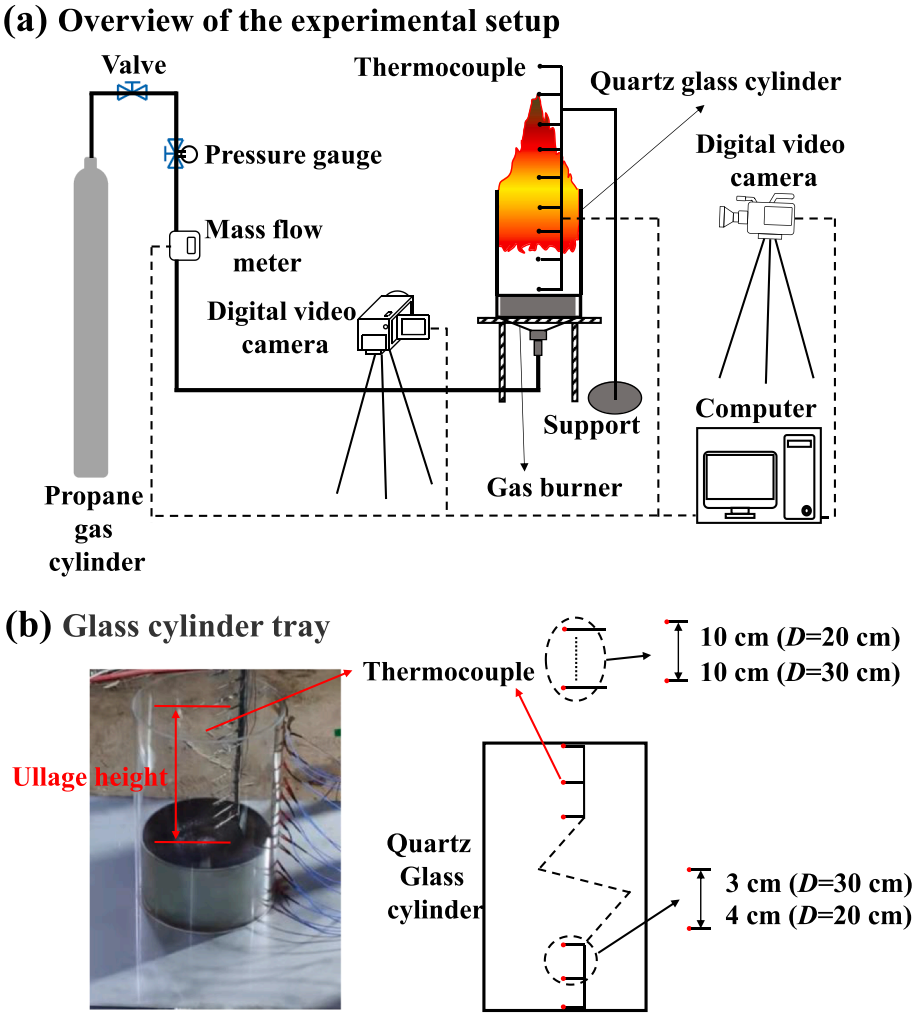

Fig. 1. Schematic of the experimental setup: (a) overview of the experimental setup; (b) glass cylinder tray.

that the axial flame temperature of free burning fires can be well predicted by existing classical or modified models. However, in practical accident cases the presence of restricted boundaries (e.g., sidewall, ceiling, ullage) can also affect the burning characteristics of the fire and flame temperature.

Tao et al. [11] conducted a series of experiments to study the effects of a wall on the temperature distributions of methane jet flames with different heat release rates (2.76 kW $\leq \dot{Q} \leq$ 8.83 kW) and nozzle inclined angles. A model for the temperature profile was developed to account for both the nozzle inclined angle and air entrainment. Zhang et al. [12] investigated the temperature profile beneath an inclined ceiling induced by gaseous jet flames (2.6 kW $\leq \dot{Q} \leq$ 9.6 kW) and a revised plume radius b_L including the ceiling inclination angle was proposed. A similar correlation was also deduced by Zhang et al. [13] for wall-attached propane jet flames (2.23 kW $\leq \dot{Q} \leq$ 19.64 kW) with different ceiling inclination angles, in which the total flame length was introduced to modify the characteristic length scale in the temperature profile model.

Compared with ceilings and walls, the air entrainment will be more restricted inside a tank with a large ullage height, which often led to the rise of the flame base, resulting in different flame characteristics [14], in which case the total flame can be considered to consist of an upper flame (outside the tank) and a down-reaching flame (inside the tank). Sharma and Mishra [15] experimentally studied the effects of the ullage height on the upper flame temperature profile using stainless steel trays (D = 5 and 10 cm) and found that the temperature of the upper flame for the cases with large ullage heights is 10–20 % higher than that for the ones with small ullage heights. Liu et al. [16] conducted heptane experiments using steel trays to investigate the effects of the ullage height ($0 \leq h/D \leq$ 1.5) on the evolution of the fire plume temperature (D = 10 and 15 cm) and noted that the centerline temperature in the upper flame increases with the ullage height ($h/D > 0.5$ for D = 15 cm, and $h/D > 0.3$ for D = 10 cm) and a model was developed by modifying the virtual origin based on physical and dimensionless analysis.

The above studies clearly indicated that the ullage height can significantly affect the flame temperature profile. However, most of these studies were based on relatively low ullage heights, which may be very different from practical fire accidents (low liquid level and large ullage height). Furthermore, these studies were focused on the temperature profile of the upper flame and that of the down-reaching flame (inside the tank) was generally not considered. To fill this knowledge gap, this study is aimed at investigating the axial temperature profile of propane diffusion flames with large ullage heights with an equal emphasis on both the upper and down-reaching flames. A series of experiments were conducted using two customized fuel trays with different ullage heights and fuel supply rates. The temperature profiles both inside and outside the fuel tray were measured and analyzed. Based on dimensionless analysis and experimental data, new correlations for the virtual origin were proposed, which were then incorporated in the predictions of the temperature profiles in both upper and down-reaching flames and validated against the experimental data.

2. Experimental setup

Fig. 1 depicts a schematic of the experimental setup. Two circular gas burners (D = 20 and 30 cm) were used. The tank sidewall was made of transparent quartz glass, so the down-reaching flame could be observed and the flame length measured. This configuration simulates the pool fire scenario after the failure of liquid fuel storage tanks. In a liquid fuel tank fire, the burning rate is affect by the heat feedback from the flame to the fuel surface [14,15], which makes it difficult to systematically study the relation between the flame temperature and the heat release rate (HRR). In comparison, with gas burners the fuel flow rate (heat release rate) can be accurately controlled by a mass flow meter (±0.01 L/min). Furthermore, the temperature profile of a gas burner flame during its steady burning stage is expected to be the same as that of a tank fire because of similar flame behaviors.

Table 1
Specification of the experimental conditions.

Test No.	Diameter of burner (cm)	h/D	Propane volume flow rate (L/min)	HRR (KW)	$Fr(u_s^2/gD)$
1–16	20	0.8/1.0/1.2/1.4	6	9.24	5.17×10^{-6}
			8	12.32	9.19×10^{-6}
			10	15.40	1.44×10^{-5}
			12	18.48	2.07×10^{-5}
17–30	30	0.8/1.0/1.2/1.4	12	18.48	2.72×10^{-6}
			16	24.64	4.84×10^{-6}
			20	30.80	7.56×10^{-6}
			24	36.96	1.09×10^{-5}

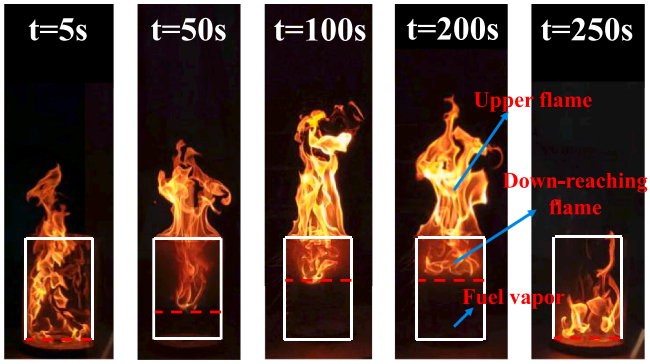

Fig. 2. Typical flame behaviour at different times for the case D = 20 cm, h = 28 cm, Q = 10 L/min.

Two video cameras at a speed of 25 frames per second were employed to record the flame behavior, based on which the flame length was calculated using a flame images processing method [17,18]. Videos of the flames were converted to a series of binary pictures and the probability of flame intermittency was then calculated. The mean flame length was determined based on a flame intermittency of 0.5 [19]. The upper flame length (L_{upper}) and the down-reaching flame length (L_{down}) refer to the vertical distances from the upper rim of the glass cylinder to the flame tip and flame base, respectively.

A series of K-type thermocouples (diameter: 1 mm, uncertainties: ±1 K) were placed along the centerline to measure the temperature of the fire plume and fuel vapor, as shown in Fig. 1(b). Estimates of the error of temperature measurement due to radiation loss by the thermocouples are provided in Appendix 1. A summary of the experimental conditions is shown in Table 1. The fuel supply flow rate ranged from 6 to 24 L/min corresponding to a maximum gas velocity (u_s) of 0.00637 m/s (for D = 20 cm), which, based on the calculated Froude number ($Fr = u_s^2/gD$), indicate that the flow was dominated by buoyancy [20]. Four dimensionless ullage heights, h/D, were used, namely 0.8, 1.0, 1.2, and 1.4, which are consistent with the ones expected in practical liquid fuel tanks from around 0.15 (full tank) to 1.4 (empty tank) [21,22]. All experiments were conducted in a quiescent environment with no wind and at atmospheric pressure. The ambient temperature was 20 ± 3℃ and the relative humidity was 54 ± 10 %. Each experiment lasted for at least 3 min after reaching the steady burning stage and was repeated at least two times to ensure the repeatability of the tests with the average results of the repeated tests used in the data analysis.

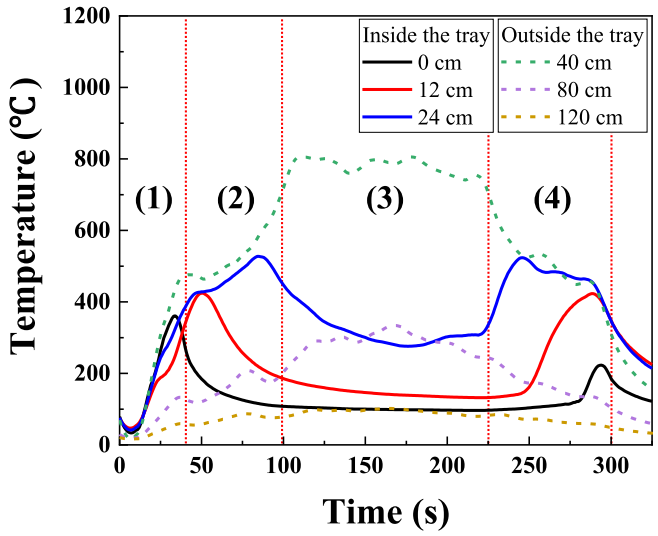

Fig. 3. Axial temperature histories at different heights for the case $D = 20$ cm, $h = 28$ cm, $Q = 10$ L/min.

3. Result and discussion

3.1. Flame behavior and temperature profile in burning process

As the axial temperature profile is closely related to the flame position and flame shape, the general flame behavior will be discussed first. Fig. 2 shows the typical flame shapes at different times (for the case $D = 20$ cm, $h = 28$ cm, $Q = 10$ L/min). Based on the position of the flame base, the whole burning process can be divided into four stages: (1) initial stage, (2) developing stage, (3) steady burning stage and (4) extinguishment stage. At the initial stage, the flame was mainly inside the tray, and the flame base was close to the burner surface because the tray was full of air to sustain burning [23]. At the developing stage, the flame base gradually moved up as the oxygen inside the tray was being consumed and the air entrainment was restricted by the large ullage height. At the steady burning stage, both the flame shape and flame length became stable, with the flame base and flame tip also relatively fixed. This indicates a balance between the air entrainment around the tray exit and the upward fuel flow. During the steady burning stage, three distinguishing regions can be observed: (1) the fuel vapor region, (2) the down-reaching flame region and (3) the upper flame region. At the extinguishment stage, the flame length gradually decreased after the fuel supply was stopped and the flame re-entered the tray just before extinguishment. It is worthwhile to note that similar flame behaviors are expected for a liquid tank fire due to the reduction of the fuel supply rate, although extinguishment would occur naturally in a liquid fuel tank fire due to complete burning of the fuel.

Fig. 3 presents the axial temperature histories at different heights (Case: $D = 20$ cm, $h = 28$ cm, $Q = 10$ L/min). At the initial stage, the temperatures both inside and outside the tray increase rapidly because the flame became full of the tray in a short time, which agrees with the observations in [24]. As burning continues, the temperatures inside the tray gradually decrease indicating a rise of the flame base. At the steady stage, the temperatures remain relatively constant, consistent with the steady flame shape and flame base position. During this stage, the maximum upper flame temperature reaches about 800℃ whereas that in the fuel vapor region is below 200℃. At the extinguishment stage, the measured temperatures inside the tray increase shortly as the flame re-entered the tray. Among the four burning stages, the steady burning stage is the most important one as it can sustain for a long time in practical accidents and the results at this stage will be further analyzed.

3.2. Axial temperature profile at steady burning stage

Fig. 4(a) shows the profile of the axial temperature at the steady stage for the case $D = 30$ cm, $h = 36$ cm and $Q = 20$ L/min. The axial temperature increases with height (Z) first, followed by a relatively constant value before it decreases with a further increase in height. In the fuel vapor region, the axial temperature increases slowly from 138 ℃ to 212℃ as the height increases from 0 to 18 cm. The flame base is located away from the burner surface. As the height continues to increase, the temperature increases sharply before reaching its maximum (about 800℃). As the height further increases, the axial temperature gradually decreases, which is consistent with the finding in [25]. Based on the flame behaviors, temperature variations and flame intermittency, five regions can be identified: 1) fuel vapor, 2) down-reaching intermittent flame, 3) continuous flame (down-reaching and upper flame), 4) upper intermittent flame and 5) buoyant plume. The boundaries of the different regions were determined by the flame intermittency values of 0.95 and 0.05, respectively [10,19], as shown Fig. 4(b).

To further demonstrate the effect of the ullage height on the temperature profile, Fig. 5(a) compares the results of two cases with different ullage heights ($h = 24$ and 42 cm) but the same burner size and fuel supply flow rate ($D = 30$ cm, $Q = 20$ L/min). It is interesting to note that, as the ullage height increases, the length of the fuel vapor region (distance between the flame base and the burner surface) increases, whereas the lengths of other regions remain nearly the same. This can be explained by the fact that the distance between the flame base and the burner rim (the down-reaching flame length) is only related to the fuel flow rate independent of the ullage height. As a result, for the same fuel supply rate the length of the fuel vapor region is mainly determined by the ullage height, as verified by a linear relation between the length of

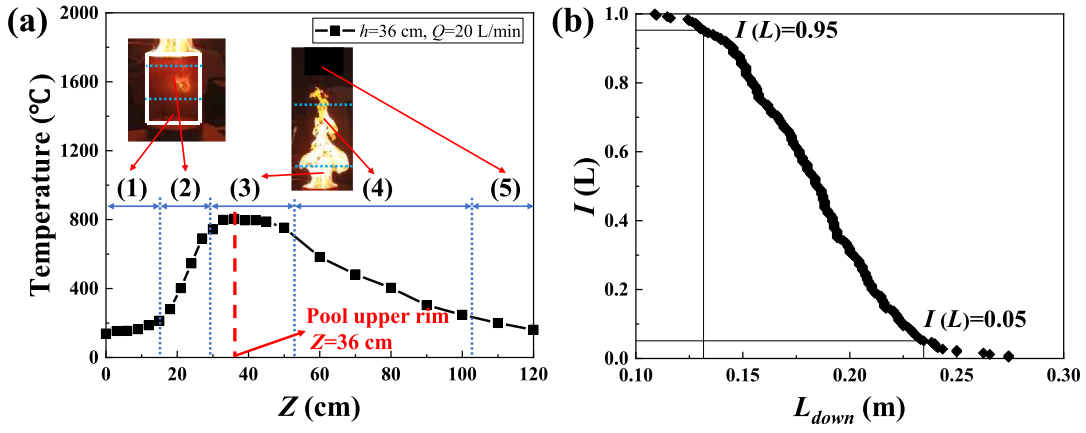

Fig. 4. (a) The steady axial temperature profile for the case $D = 30$ cm, $h = 36$ cm, $Q = 20$ L/min, (b) determination of the flame intermittencies of the boundaries.

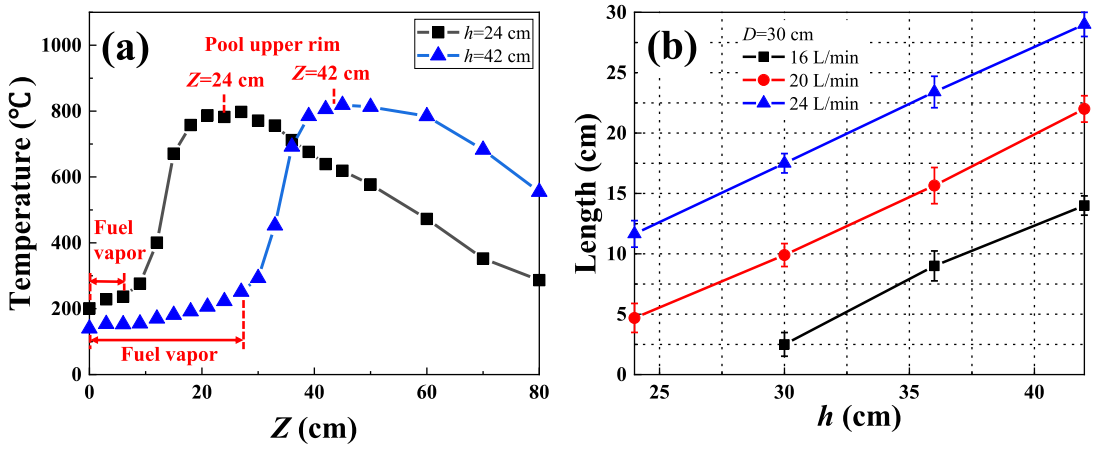

Fig. 5. (a) Comparison of the axial temperature profile between two cases with different ullage heights ($D = 30$ cm, $Q = 20$ L/min). (b) The length of the fuel vapor region as a function of the ullage height.

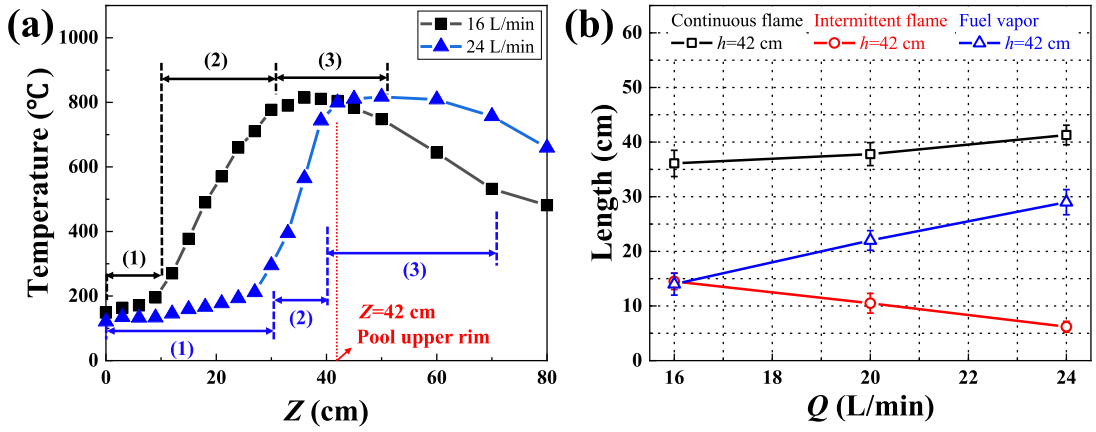

Fig. 6. (a) Comparison of the axial temperature profile between two cases with different fuel supply rates ($D = 30$ cm, $h = 42$ cm). (b) The lengths of different regions as a function of the fuel flow rate.

the fuel vapor region and the ullage height, as shown in Fig. 5(b) applicable for all the cases.

As the axial temperature is closely related to the flame shape, we can expect that the fuel supply rate also affects the axial temperature profile, as shown in Fig. 6(a), which compares the results of the two cases with different fuel supply rates ($Q = 16$ and 24 L/min) but the same burner diameter and ullage height ($D = 30$ cm, $h = 42$ cm). As the fuel supply rate increases, the length of the fuel vapor region gradually increases whereas that of the down-reaching intermittent flame region decreases. This can be explained by the fact that the flame base position is controlled by the competition of the downward momentum of air entrainment and the upward momentum of the fuel gas. For a large fuel supply rate, the upward momentum of fuel gas can overcome the downward momentum of air entrainment, leading to the rise of the flame base. Furthermore, it can be observed that the length of the continuous flame region increases with the fuel supply rate, as shown in Fig. 6(b), which presents the variation of the lengths of different regions as a function of the fuel flow rate.

3.3. Axial temperature profile model

3.3.1. Upper flame temperature profile

For a buoyant diffusion flame, McCaffrey [6] proposed the following correlation for the axial temperature rise above ambient, ΔT:

Table 2
Parameters of McCaffrey [6] and Cox and Chitty [26] model.

Regions/Authors	McCaffrey [6]		Cox and Chitty [26]	
	κ	η	κ	η
Continuous flame	6.84	1/2	6.83	1/2
Intermittent flame	1.93	0	1.85	0
plume	1.12	−1/3	1.08	−1/3

$$\Delta T = T_\infty \left(\frac{\kappa}{C\sqrt{2g}}\right)^2 \left(\frac{Z}{\dot{Q}^{2/5}}\right)^{2\eta-1} \quad (1)$$

where Z is the vertical height above the burner, C is a constant and equals 0.9, T_∞ is the ambient air temperature, g is the gravitational acceleration, and $\dot{Q}$ is the heat release rate. A similar equation of ΔT *vs* $Z/\dot{Q}^{2/5}$ was also given by Cox and Chitty [26]. The empirical coefficients κ and η for both models are shown in Table 2.

Fig. 7 shows a comparison of measured temperature rises and the ones calculated by both models. It can be found that both models generally overestimate the temperature rise, especially for the cases with small fuel supply flow rates (large down-reaching flame length). The reasons are twofold. On the one hand, as some combustion occurred inside the fuel tray, the heat release rate of the upper flame ($\dot{Q}_{upper}$) is smaller than the total heat release rate ($\dot{Q}$), leading to lower values of $Z/$

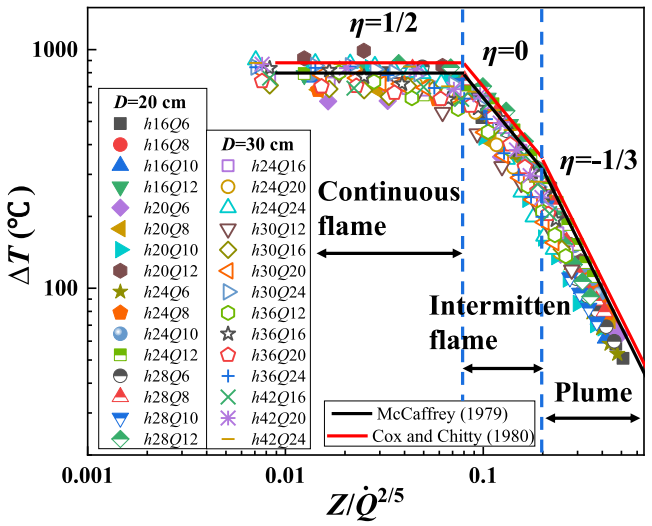

Fig. 7. Comparisons between the experimental axial temperature and the predictive results.

$\dot{Q}^{2/5}$ in the experiments (i.e., the experimental data is less than the model prediction). On the other hand, the fire virtual origin was not considered in the calculations, which could also lead to an over-estimation of the flame temperature [9].

The virtual origin can be used to account for different buoyancy fluxes at the source and is generally expressed as a function of the burner size and heat release rate [27]. For a given heat release rate, the thermal buoyancy flux is mainly determined by the burner area (gas vent area) [28]. As a result, the virtual origin varies with the buoyancy flux and can be calculated using the axial temperature in the plume [29,30].

In the plume, the axial temperature can be expressed as [29,31]:

$$\Delta T = \frac{5}{6}\left(\frac{9\pi^2\alpha^4}{10}\right)^{-1/3} g^{-1/3}\left(\rho_\infty c_p T_\infty\right)^{-2/3}\dot{Q}_c^{2/3} Z^{-5/3} \tag{2}$$

where α is the entrainment rate coefficient, ρ_∞ is the ambient density, and $\dot{Q}_c$ is the convective heat release rate ($\dot{Q}_c$ is about 60 %–80 % of the total heat release rate and in this study 70 % was used [23,32]).

Based on dimensionless analysis, Eq. (2) can be simplified as:

$$\frac{\Delta T}{T_\infty} = A\alpha^{-4/3}\left(\frac{\dot{Q}}{\rho_\infty c_p T_\infty g^{1/2} D^{5/2}}\right)^{2/3}\left(\frac{Z}{D}\right)^{-5/3} \tag{3}$$

where A is a constant.

By considering the virtual origin and replacing Z with $(Z - Z_0)$, Eq. (3) becomes [33]:

$$\frac{\Delta T/T_\infty}{\dot{Q}^{*2/3}} = fun\left(\frac{Z - Z_0}{D}\right) \tag{4}$$

where the dimensionless heat release rate $\dot{Q}^* = \frac{\dot{Q}}{\rho_\infty c_p T_\infty g^{1/2} D^{5/2}}$.

Eq. (4) can be further expressed as:

$$\left(\frac{\dot{Q}^{*2/3}}{\Delta T/T_\infty}\right)^{3/5} \propto Z - Z_0 \tag{5}$$

Eq. (5) implies that (i) there exists a linear relation between $\left(\frac{\dot{Q}^{*2/3}}{\Delta T/T_\infty}\right)^{3/5}$ and Z and (ii) by plotting $\left(\frac{\dot{Q}^{*2/3}}{\Delta T/T_\infty}\right)^{3/5}$ against Z, the virtual origin can be found from the intercept of the linear fit and the x-axis. It is noted that the effect of the down-reaching flame is considered in the virtual origin. Fig. 8 show the results for the cases at different fuel flow rates with $D = 20$ cm and $h = 20$ cm, which verifies that $\left(\frac{\dot{Q}^{*2/3}}{\Delta T/T_\infty}\right)^{3/5}$ increases linearly with Z. The determined virtual origin values are negative for most cases and increase with an increase of the fuel flow rate (i.e., heat release rate). This could be partly due to the fact that the down-reaching flame length decreases with an increase of the heat release rate.

The virtual origin height is related to the heat release rate, flame temperature rise and fire diameter [10]:

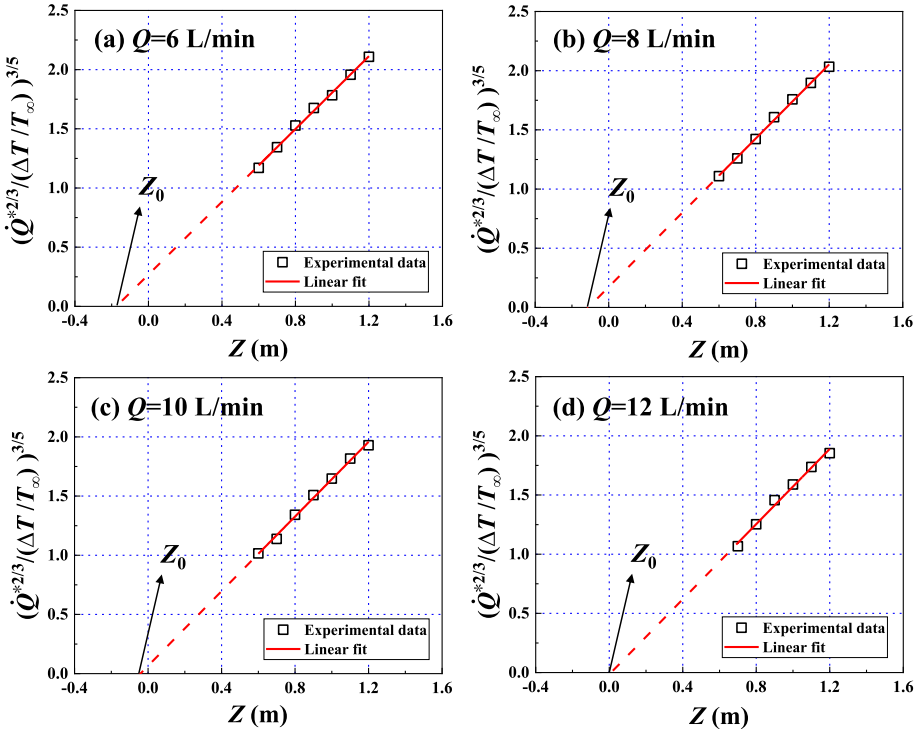

Fig. 8. Determination of virtual origins for the cases with different fuel flow rates ($D = 20$ cm and $h = 20$ cm).

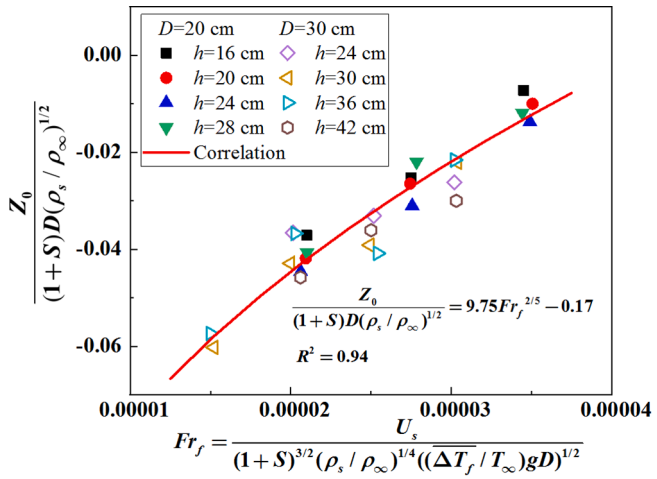

Fig. 9. Correlation of dimensionless virtual origin height and flame Froude number.

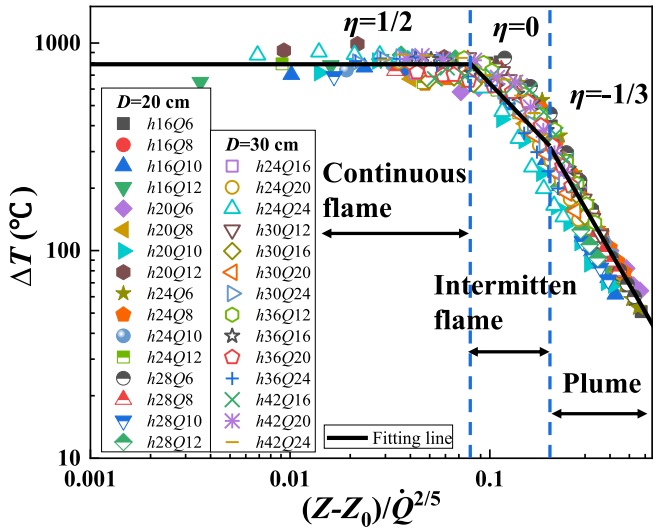

Fig. 10. Correlation of the axial temperature of the upper flame and $(Z - Z_0)/\dot{Q}^{2/5}$.

$$Z_0 = fun\left(\dot{Q},\ \Delta T_f,\ D\right) \tag{6}$$

Based on the experimental data and dimensionless analysis [8,9], Eq. (6) can be rewritten as:

$$Z_0 = \alpha \dot{Q}^{2/5} + \beta D \tag{7}$$

where α and β are model coefficients. It is noted that:

$$\frac{Z_0}{D} \propto \left(\frac{\dot{Q}}{\sqrt{D^5}}\right)^{2/5} \propto \left(\frac{u_s}{\sqrt{D}}\right)^{2/5} \propto \left(\sqrt{Fr}\right)^{2/5} \tag{8}$$

where u_s is the fuel gas velocity and Fr is the Froude number ($Fr = u_s^2/gD$). A global flame Froude number including the fuel property and environmental factors effects is provided to describe the virtual origin height [34]:

$$Fr_f = \frac{u_s}{(1+S)^{3/2} D(\rho_s/\rho_\infty)^{1/4}\left((\overline{\Delta T_f}/T_\infty)gD\right)^{1/2}} \tag{9}$$

where ρ_s is the fuel density, $\overline{\Delta T_f}$ is the mean maximum flame temperature rise, and S is the air to fuel mass stoichiometric ratio. Based on Eqs. (8) and (9), a dimensionless virtual origin can be defined as:

$$\frac{Z_0}{(1+S)D(\rho_s/\rho_\infty)^{1/2}} \propto Fr_f^{2/5} \tag{10}$$

The correlation between the dimensionless virtual origin height and the flame Froude number is shown in Fig. 9. It can be observed that the dimensionless virtual origin height increases with Fr_f, which agrees well with the observation in [10]. By fitting the experimental data, the following correlation can be determined:

$$\frac{Z_0}{(1+S)D(\rho_s/\rho_\infty)^{1/2}} = 9.75Fr_f^{2/5} - 0.17 \tag{11}$$

With the virtual origin height Z_0 calculated from Eq. (11), we can now plot the temperature rise ΔT against $(Z - Z_0)/\dot{Q}^{2/5}$ as shown in Fig. 10. The data converges well for all the cases with different ullage heights and heat release rates.

The final axial temperature profile of the upper flame is given in Eq. (12), where it can be noted that both the boundary values and the exponents in all three regions agree well with those reported by McCaffrey [6] and Cox and Chitty [26].

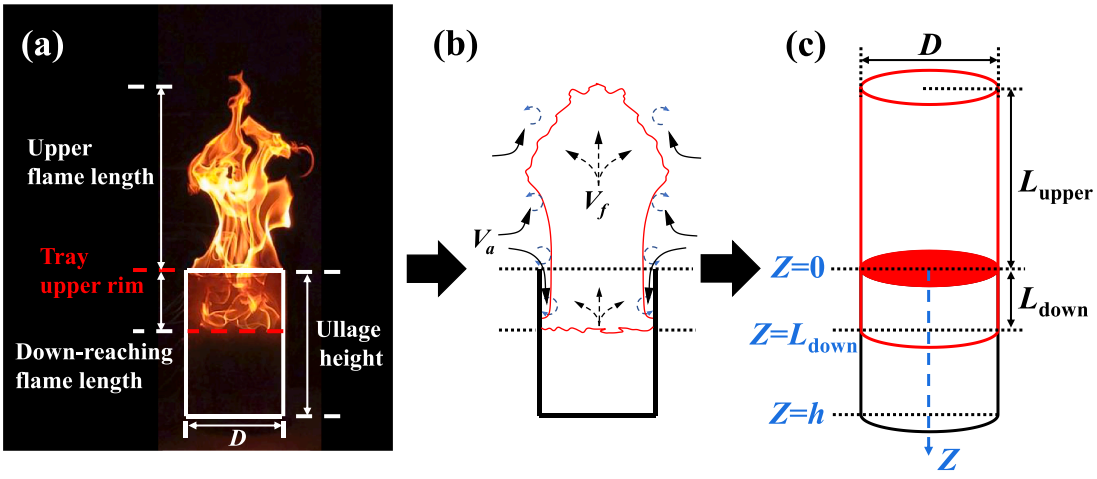

Fig. 11. The schematic diagram of the flame shape assumption.

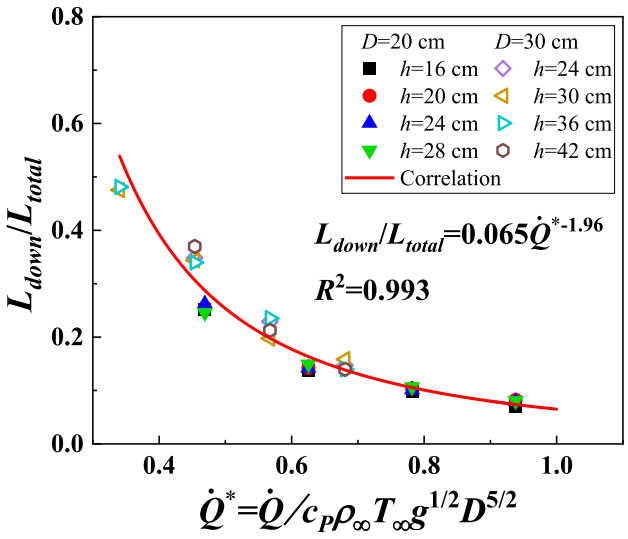

Fig. 12. Correlation of L_{down}/L_{total} and $\dot{Q}^*$.

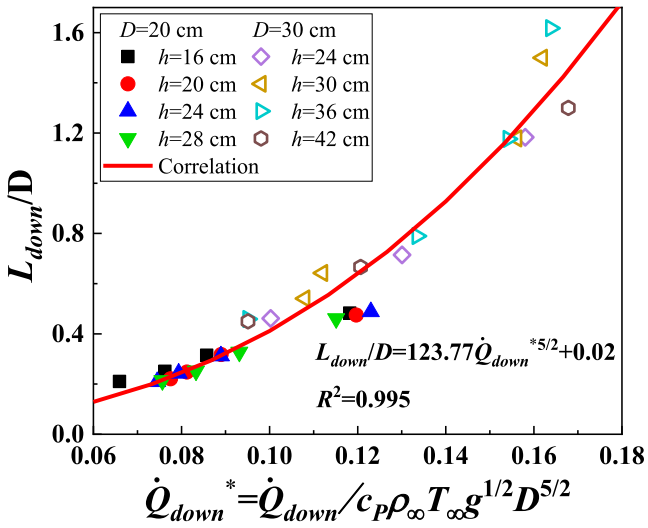

Fig. 13. Correlation of dimensionless down-reaching flame length and dimensionless heat release rate.

$$\Delta T=\begin{cases}790.44,\ \left(\dfrac{Z-Z_0}{\dot{Q}^{2/5}}\right)\leqslant 0.08,\ \text{continuous zone}\\ 63.88\left(\dfrac{Z-Z_0}{\dot{Q}^{2/5}}\right)^{-1},\ 0.08<\left(\dfrac{Z-Z_0}{\dot{Q}^{2/5}}\right)\leqslant 0.2,\ \text{intermittent zone}\\ 20.63\left(\dfrac{Z-Z_0}{\dot{Q}^{2/5}}\right)^{-5/3},\ \left(\dfrac{Z-Z_0}{\dot{Q}^{2/5}}\right)>0.2,\ \text{plume zone}\end{cases} \tag{12}$$

3.3.2. Down-reaching flame temperature profile

From the temperature profile of the down-reaching flame shown in Fig. 3, three regions can be identified, similar to those for the upper flame. For further analysis, the total flame is assumed to be from two fire sources with the total heat release rate ($\dot{Q}$ or $\dot{Q}_{total}$) consisting of an upper heat release rate ($\dot{Q}_{upper}$) and a down-reaching heat release rate ($\dot{Q}_{down}$).

The shape of the steady flame is simplified as a cylinder with the flame diameters of both upper and down-reaching flames the same as the tray diameter [14,35], as shown in Fig. 11. Furthermore, the combustion in both upper and down-reaching flames is assumed to be uniform [36,37] so the heat release rate is proportional to the flame volume.

The heat release rate of the down-reaching flame ($\dot{Q}_{down}$) can now be determined as:

$$\dot{Q}_{down}=\frac{V_{down}}{V_{total}}\dot{Q}_{total}=\frac{L_{down}}{L_{total}}\dot{Q} \tag{13}$$

where V_{down} and V_{total} are the volumes of the down-reaching and total flames, respectively.

In order to estimate$\dot{Q}_{down}$, we need to obtain the flame length ratio L_{down}/L_{total}. As shown in Fig. 6, with an increase of the fuel supply rate the base of the flame gradually moves up, resulting in a decrease of the down-reaching flame length while an increase of the upper flame length, i.e., a decrease of L_{down}/L_{total}. As the ratio L_{down}/L_{total} is also related to the burner size and air entrainment, the normalized HRR,$\dot{Q}^*$, can be used to correlate L_{down}/L_{total} as done in [30]. Fig. 12 plots L_{down}/L_{total} against $\dot{Q}^*$ for all the tests with different tray diameters, heat release rates and ullage heights, and all the data collapse into a single line with the following correlation.

$$L_{down}/L_{total}=0.065\dot{Q}^{*-1.96} \tag{14}$$

By combining Eq. (13) and Eq. (14), we note that $\dot{Q}_{down}$ is a function of the total heat release rate ($\dot{Q}$) and tray diameter (D), independent of the ullage height and burner diameter.

The flame length is closely related to the tray diameter, heat release rate, density of ambient air, acceleration of gravity, air specific heat at constant pressure, and ambient temperature [17,38]. As the down-reaching flame is simplified as an independent fire source, the corresponding flame length can be expressed as:

$$L_{down}=fun\left(D,\ \dot{Q}_{down},\ \rho_\infty,\ g,\ c_p,\ T_\infty\right) \tag{15}$$

Based on dimensionless analysis [38], the dimensionless flame height (L_{down}/D) can be correlated with the dimensionless heat release rate ($\dot{Q}^*_{down}=\frac{\dot{Q}_{down}}{\rho_\infty c_p T_\infty g^{1/2}D^{5/2}}$) as:

$$\frac{L_{down}}{D}=A\left(\dot{Q}^*_{down}\right)^n+B \tag{16}$$

Fig. 13 shows the correlation between L_{down}/D and $\dot{Q}^*_{down}$ for all the cases with different fuel flow rates, tray sizes and ullage heights. It can be noted all the data can be represented with the same correlation given in Fig. 13 and Eq. (17). This result also verifies the validity of the use of the ratio of the flame lengths in Eq. (13) to calculate the heat release rate of the down-reaching flame.

$$\frac{L_{down}}{D}=123.77\left(\dot{Q}^*_{down}\right)^{5/2}+0.02 \tag{17}$$

To develop a model for the axial temperature of the down-reaching flame, the virtual origin height of the down-reaching flame can be found following [9,39]:

$$Z_0=L_{down}-Eb_L \tag{18}$$

where E is a dimensionless constant equal to 5.9 [9] and b_L is the radius of the fire plume at the flame length, which can be obtained from integration of the convective-heat flux over the plume cross section as:

$$b_L=\left[2\pi\beta\xi\left(c_p\rho_\infty\right)^{4/5}T_\infty^{3/5}g^{2/5}\right]^{-1/2}\dot{Q}_{c,down}^{2/5}T_{mL}^{1/2}\Big/\Delta T_{mL}^{3/5} \tag{19}$$

where T_{mL} and ΔT_{mL} is the axial temperature and excess axial temperature above ambient at the mean flame length, respectively, $\dot{Q}_{c,down}$ is the convective heat release rate of the down-reaching flame, ξ is an invariant dimensionless parameter having a value of 2.2 [40,41] and β is

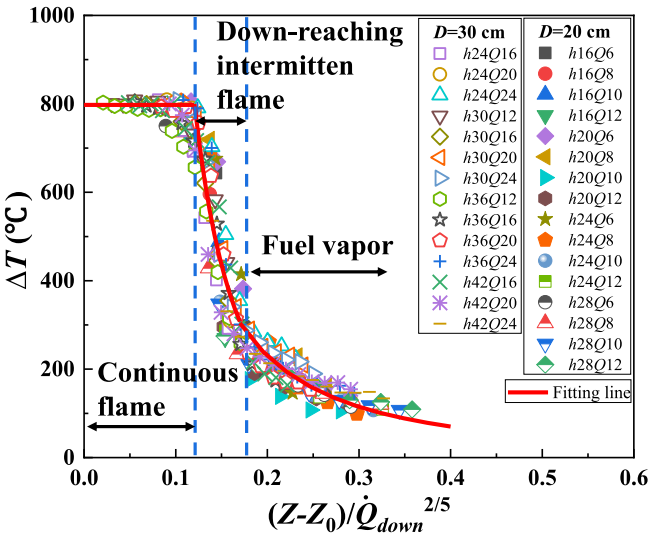

Fig. 14. Correlation of the axial temperature profile of the down-reaching flame and $(Z - Z_0)/\dot{Q}_{down}^{2/5}$.

a dimensionless constant equal to 0.41 [9].

Combining Eqs. (17)–(19), the virtual origin height for the down-reaching flame can be calculated as:

$$\frac{Z_0}{D} = 123.77\left(\dot{Q}^*_{down}\right)^{5/2} + 0.02 - E\left[2\pi\beta\xi\left(c_p\rho_\infty\right)^{4/5}T_\infty^{3/5}g^{2/5}\right]^{-1/2}\frac{T_{mL}^{1/2}\dot{Q}_{c,down}^{2/5}}{\Delta T_{mL}^{3/5}D} \tag{20}$$

Similar to the upper flame, we can now plot in Fig. 14 for the down-reaching flame the temperature rise ΔT against $(Z - Z_0)/\dot{Q}_{down}^{2/5}$, where Z is the distance from inside of the tray to the burner rim and Z_0 is calculated from Eq. (20).

Three regions corresponding to the down-reaching continuous flame, intermittent flame, and fuel vapor regions can be clearly identified, consistent with those observed for the upper flame. The axial temperature in the down-reaching continuous flame region is nearly constant, decreases quickly in the intermittent region and remains relatively low in the fuel vapor region.

It can be seen in Fig. 14 that all the data collapse and the final correlations for the axial temperature distribution in the down-reaching flame region can be obtained as shown in Eq. (21). It is worthwhile to note that the model predicts well the axial temperature of the down-reaching flame for the cases with a wide range of ullage heights from 16 to 42 cm.

$$\Delta T = \begin{cases} 797.49, \left(\dfrac{Z - Z_0}{\dot{Q}_{down}^{2/5}}\right) \leqslant 0.12, \textit{continuous zone} \\ 2.25\left(\dfrac{Z - Z_0}{\dot{Q}_{down}^{2/5}}\right)^{-2.78}, 0.12 < \left(\dfrac{Z - Z_0}{\dot{Q}_{down}^{2/5}}\right) \leqslant 0.17, \textit{intermittent zone} \\ 14.63\left(\dfrac{Z - Z_0}{\dot{Q}_{down}^{2/5}}\right)^{-1.71}, \left(\dfrac{Z - Z_0}{\dot{Q}_{down}^{2/5}}\right) > 0.17, \textit{fuel vapor zone} \end{cases} \tag{21}$$

4. Conclusion

This study was aimed at experimentally investigating the axial temperature profile of turbulent diffusion flames with large ullage heights. Experiments were performed with different fuel tray sizes, fuel flow rates and ullage heights. Axial temperature in both upper and down-reaching flames were measured and analyzed, based on which new correlations for the virtual origin height were deduced and subsequently incorporated in the models for the prediction of the axial temperature. The main results are as follows:

(1) The whole burning process can be characterized by four stages: 1) initial stage, 2) developing stage, 3) steady burning stage and 4) extinguishment stage. At the initial stage, the flame length and corresponding temperature increased rapidly as more fuel is being consumed. As burning continued, the flame base gradually moved up before becoming relatively fixed with a relatively constant temperature profile. At the extinguishment stage, the flame re-entered the fuel tray after the fuel supply was stopped, resulting in an increase of the temperature of the down-reaching flame.

(2) The axial temperature profile at the steady stage was found to depend on both the ullage height and fuel supply rate. Based on the flame behaviors and flame intermittencies, the axial temperature profile was divided into five regions: 1) fuel vapor, 2) down-reaching intermittent flame, 3) continuous flame (down-reaching and upper flame), 4) upper intermittent flame and 5) buoyant plume. For a given fuel supply rate, the length of the fuel vapor region showed a linear relation with the ullage height. As the fuel supply rate increased, the length of the fuel vapor and continuous flame regions gradually increased whereas that of the down-reaching intermittent flame region showed an opposite trend.

(3) Existing models developed for pool fires tended to overestimate the axial temperature of the upper flame because the down-reaching flame was not considered. A new virtual origin model considering the effects of the tray size and air entrainment was proposed, which was found to correlate well with the flame Froude number (Fr_f). Based on the virtual origin model, a global correlation was developed to predict the axial temperature of the upper flame.

(4) For the down-reaching flame, three regions corresponding to down-reaching continuous flame, intermittent flame, and fuel vapor regions were identified according to the axial temperature variations and flame intermittencies. A virtual origin model was developed, based on which a new piecewise function was established to estimate the axial temperature of the down-reaching flame and validated against the experimental data for cases with different ullage heights.

The present experimental results provide insights into the axial temperature profile with large ullage heights, which can enrich the basic experimental data, particularly for the down-reaching flame. Moreover, the fundamental analysis and corresponding models will enhance the understanding of the temperature profile and thus be of practical use in thermal hazard assessment of fire accidents involving tank liquid fuels. Finally, it should be mentioned that in liquid tank fires the heat feedback from the flame can play a significant role in fire development. In this work, gas burners were used to decouple the flame heat feedback and burning rate, allowing us to systematically study of the effects of the ullage height on the flame temperature profile during the steady burning stage. Experiments are planned to be conducted for large-scale liquid fuel tank fires, and the data will be used to further validate the models developed in this work.

CRediT authorship contribution statement

Jinlong Zhao: Methodology, Validation, Funding acquisition, Investigation, Supervision, Writing – original draft, Writing – review & editing. **Xiang Zhang:** Data curation, Investigation, Writing – original draft. **Guangheng Song:** Data curation, Writing – review & editing. **Hong Huang:** Supervision, Writing – review & editing. **Jianping Zhang:** Conceptualization, Methodology, Supervision, Writing – review & editing.

Declaration of Competing Interest

The authors declare that they have no known competing financial

interests or personal relationships that could have appeared to influence the work reported in this paper.

Data availability

Data will be made available on request.

Acknowledgements

This study was sponsored by the National Natural Science Foundation of China (No. 72091512 and No. 51906253), the Fundamental Research Funds for the Central Universities (No. 2020QN05 and No. 2021JCCXAQ01).

Appendix

The radiation correction of thermocouple in this work is referred to the method adopted by Cox and Chitty [42] and Dupuy et al. [43]. The difference in mean temperature between the surrounding gas and the thermocouple in the flame gas flow is given, to first order, by

$$\Delta T = \frac{\sigma\varepsilon_{th}\left(1-\varepsilon_g\right)T_g^4}{h_c + 4\sigma\varepsilon_{th}T_g^3} \tag{A1}$$

Where ΔT_r is the temperature measurement error, T_g is the averaged surrounding gas temperature, σ is the Stefan-Boltzmann constant, h_c is the convective heat transfer coefficient, ε_{th} and ε_g are the emissivity of the thermocouple and the surrounding gas, respectively.

As indicated by Cox and Chitty [42], the convective heat transfer coefficient for a cylinder can be assumed to be:

$$h_c = \frac{k}{d_{th}}Nu = \frac{k}{d_{th}}\left(0.43 + 0.53Re^{0.5}Pr^{0.31}\right) \tag{A2}$$

where k is the thermal conductivity of the gas, d_{th} is the thermocouple's diameter, Nu is the Nusselt number for heat exchange between the thermocouples and the gas flow, Re and Pr are the Reynolds and Prandtl numbers for the gas flow.

According to the study of Fischer et al. [44], Re can be expressed as:

$$Re = \frac{\overline{u}d_{th}}{v} \tag{A3}$$

where v is the kinematic viscosity of the gas, $\overline{u}$ is the mean surrounding gas velocity, which given as [44]:

$$\overline{u} = \left[gD\left(T_g - T_\infty\right)/T_\infty\right]^{1/2} \tag{A4}$$

Assuming that the gas emissivity inside the flame is 0.1 and the thermocouple's emissivity is 0.9 [42,43], the radiation error and characteristic response time were calculated for various burner sizes and temperatures. The results were reported in Table A1.

It can be found that the radiation error increases with the gas temperature. For T_g= 500 K in plume zone, the radiation errors are less than 20 K, which indicates that the radiation error can be ignored for low gas temperatures. However, For T_g= 993 K in continuous flame zone, the radiation errors are larger than 112 K.

Table A1
Radiation error of thermocouples.

D (cm)	T_g (K)	$\overline{u}$(m/s)	d_{th} (mm)	Error (K)	Error (%)[a]
20	500	1.2	1.0	18	8.7
20	613	1.5	1.0	33	10.3
20	893	2	1.0	92	15.3
20	993	2.3	1.0	118	16.9
30	500	1.4	1.0	17	8.2
30	613	1.8	1.0	31	9.7
30	893	2.5	1.0	87	14.5
30	993	2.8	1.0	112	16.0

[a] Absolute error/(T_g-293).

References

[1] Deng L, Tang F, Wang XK. Uncontrollable combustion characteristics of energy storage oil pool: Modelling of mass loss rate and flame merging time of annular pools. Energy 2021;224:120181.
[2] Zhao XR, Al-Abdrabalnabi R, Wu YS, Zhou XM. Evaluations of the feasibility of oil storage in depleted petroleum reservoirs through experimental modelling studies. Fuel 2021;294:120316.
[3] Yu L, Wan H, Gao Z, Ji J. Study on flame merging behavior and air entrainment restriction of multiple fires. Energy 2021;218:119470.
[4] Liu CX, Ding L, Jangi M, Ji J, Yu LX, Wan HX. Experimental study of the effect of ullage height on flame characteristics of pool fires. Combust Flame 2020;216:245–55.
[5] Zhao JL, Zhu HQ, Zhang JP, Huang H, Yang R. Experimental study on the spread and burning behaviors of continuously discharge spill fires under different slopes. J Hazard Mater 2020;392:122352.
[6] McCaffrey BJ. Purely buoyant diffusion flames: some experimental results. NBSIR 79-1910, National Bureau of Standards, Washington, DC; 1979.
[7] Gong CZ, Ding L, Wan HX, Ji J, Gao ZH, Yu LX. Spatial temperature distribution of rectangular n-heptane pool fires with different aspect ratios and heat fluxes received by adjacent horizontal targets. Fire Saf J 2020;112:102959.
[8] Heskestad G. Engineering relations for fire plumes. Fire Saf J 1984;7:25–32.
[9] Heskestad G. Virtual origins of fire plumes. Fire Saf J 1983;5:109–14.
[10] Hu LH, Wang Q, Tang F, Delichatsios M, Zhang XC. Axial temperature profile in vertical buoyant turbulent jet fire in a reduced pressure atmosphere. Fuel 2013;106:779-786.
[11] Tao CF, Qian YJ, Tang F, Wang Q. Experimental investigations on temperature profile and air entrainment of buoyancy-controlled jet flame from inclined nozzle bounded the wall. Appl Therm Eng 2017;111:510–5.
[12] Zhang XC, Tao HW, Zhang ZJ, Tang F, Su GK, Chen S, et al. Temperature profile beneath an inclined ceiling induced by plume impingement of gas fuel jet flame. Fuel 2018;223:408–13.
[13] Zhang XL, Shi CL, Hu LH. Temperature profile of impingement flow in the corner between wall and inclined ceiling induced by gaseous fuel jet flame. Fuel 2020;259:116232.
[14] Zhao JL, Zhang X, Zhang JP, Wang W, Chen CK. Experimental study on the flame length and burning behaviors of pool fires with different ullage heights. Energy 2022;246:123397.
[15] Sharma A, Mishra KB. Experimental set-up to measure the maximum mass burning rate of storage tank fires. Process Saf Environ Prot 2019;131:282–91.
[16] Liu CX, Ding L, Ji J. Experimental study of the effects of ullage height on fire plume centerline temperature with a new virtual origin model. Process Saf Environ Prot 2021;146:961–7.
[17] Hu LH, Wang Q, Delichatsios M, Tang F, Zhang XC, Lu SX. Flame height and lift-off of turbulent buoyant jet diffusion flames in a reduced pressure atmosphere. Fuel 2013;109:234–40.
[18] Zhao JL, Wang SS, Zhang JP, Zhou R, Yang R. Experimental study on the burning characteristics of transformer oil pool fires. Energy Fuels 2020;34:4967–76.

[19] Zukoski EE, Cetegen BM, Kubota T. Visible structure of buoyant diffusion flames. Symp (Int) Combust 1985;20:361–6.
[20] Delichatsios MA. Transition from momentum to buoyancy-controlled turbulent jet diffusion flames and flame height relationships. Combust Flame 1993;92(4):349–64.
[21] Hosseinzadeh N, Kazem H, Ghahremannejad M, Ahmadi E, Kazem N. Comparison of API650-2008 provisions with FEM analyses for seismic assessment of existing steel oil storage tanks. J Loss Prev Process Ind 2013;26:666–75.
[22] API. 650 Welded Tanks for Oil Storage. thirteenth ed. Washington, DC: API Publishing Services; 2020.
[23] Liu CX, Jangi M, Ji J, Yu LX, Ding L. Experimental and numerical study of the effects of ullage height on plume flow and combustion characteristics of pool fires. Process Saf Environ Prot 2021;151:208–21.
[24] Tao Y, Lu KH, Chen XF, Mao SH, Ding YM, Zhao YS. Experimental investigation on the temperature profile of large scale RP-5 aviation kerosene pool fire in an open space. Fuel 2020;264:116852.
[25] Dupuy JL, Maréchal J, Morvan D. Fires from a cylindrical forest fuel burner: combustion dynamics and flame properties. Combust Flame 2003;135:65–76.
[26] Cox G, Chitty R. A study of the deterministic properties of unbounded fire plumes. Combust Flame 1980;39:191–209.
[27] Rouse H, Yih CS, Humphreys HW. Gravitational convection from a boundary source. Tellus 1952;4:201–10.
[28] Lu ZK, Gao YK, Li GC, Liu B, Xu Y, Tao CF, et al. The analysis of temperature and air entrainment rate for the turbulence diffusion jet flame of propane and carbon dioxide gas mixture. Energy 2022;254:124232.
[29] Karlsson B, Quintiere JG. Enclosure fire dynamics. Florida: CRC Press LLC; 1999.
[30] Wan HX, Yu LX, Ji J. Experimental study on vertical temperature distribution of symmetry axis of two identical rectangular pool fires with long sides parallel. Fire Saf J 2021;120:103044.
[31] Quintere JG. Fundamentals of fire phenomenon. England: John Wiley & Sons Ltd.; 2006.
[32] Tewarson A. Physico-chemical and combustion/pyrolysis properties of polymeric materials. Washington, DC: National Bureau of Standards; 1982.
[33] Heskestad G. Fire Plumes, Flame Height, and Air Entrainment. SFPE Handbook of Fire Protection Engineering, fifth ed., National Fire Protection Association, Quincy, MA, 2016.
[34] Delichatsios MA. Transition from momentum to buoyancy-controlled turbulent jet diffusion flames and flame height relationships. Combust Flame 1993;92:349–64.
[35] Zhuang L, Lu SX, Sun ZY, Wang JH, Kang QS. Study of flame height of aviation fuel pool fires. J China Univ Sci Technol 2009;39:763-768.
[36] Quintiere JG, Grove BS. A unified analysis for fire plumes. Symp (Int) Combust 1998;27:2757–66.
[37] Wan HX, Gao ZH, Ji J, Wang LZ, Zhang YM. Experimental study on merging behaviors of two identical buoyant diffusion flames under an unconfined ceiling with varying heights. Proc Combust Inst 2019;37:3899–907.
[38] He PX, Wang P, Wang K, Liu XP, Wang CM, Tao CF, et al. The evolution of flame height and air flow for double rectangular pool fires. Fuel 2019;237:486–93.
[39] Heskestad G. Peak gas velocities and flame heights of buoyancy-controlled turbulent diffusion flames. Symp (Int) Combust 1981;18:951–60.
[40] Kung HC, Stavrianidis P. Buoyant plumes of large-scale pool fires. Symp (Int) Combust 1982;19:905–12.
[41] Heskestad G. Turbulent jet diffusion flames: consolidation of flame height data. Combust Flame 1999;118:51–60.
[42] Cox G, Chitty R. Some source-dependent effects of unbounded fires. Combust Flame 1985;60:219–32.
[43] Dupuy J, Marechal J, Morvan D. Fires from a cylindrical forest fuel burner: combustion dynamics and flame properties. Combust Flame 2003;135:65-76.
[44] Fischer SJ, Hardouin-Duparc B, Grosshandler WL. The structure and radiation of an ethanol pool fire. Combust Flame 1987;70:291-306.